Anisotropic Phase-Field Model with Focused Latent-Heat Release

Beneš, Michal
2000

INSTITUTE OF COMPUTER SCIENCE

ACADEMY OF SCIENCES OF THE CZECH REPUBLIC

ANISOTROPIC PHASE-FIELD MODEL WITH FOCUSED LATENT-HEAT RELEASE

Michal Beneš

Technical report No. 803

January 2000

Institute of Computer Science, Academy of Sciences of the Czech Republic
Pod vodárenskou věží 2, 182 07 Prague 8, Czech Republic
phone: (+4202) 6884244 fax: (+4202) 8585789
e-mail: uivt@uivt.cas.cz

INSTITUTE OF COMPUTER SCIENCE

ACADEMY OF SCIENCES OF THE CZECH REPUBLIC

ANISOTROPIC PHASE-FIELD MODEL WITH FOCUSED LATENT-HEAT RELEASE

Michal Beneš[1]

Technical report No. 803
January 2000

Abstract

In the article, we present an anisotropic version of the phase-field system of equations with efficient coupling arising in modelling of microstructure growth in solidification of pure crystallic materials. The anisotropy is introduced into the model using the concept of Finsler geometry, applied previously by other authors. The model is studied from point of view of existence and uniqueness via a semi-discrete scheme. We give a brief information about the asymptotical behaviour of the solution. Finally, we summarize computational results situated even beyond the scope of the theory - the model is able to work in case of non-convex anisotropy.

Keywords

[1]Department of Mathematics, FNSPE, Czech Technical University of Prague, and Institute of Computer Science, Academy of Sciences of the Czech Republic

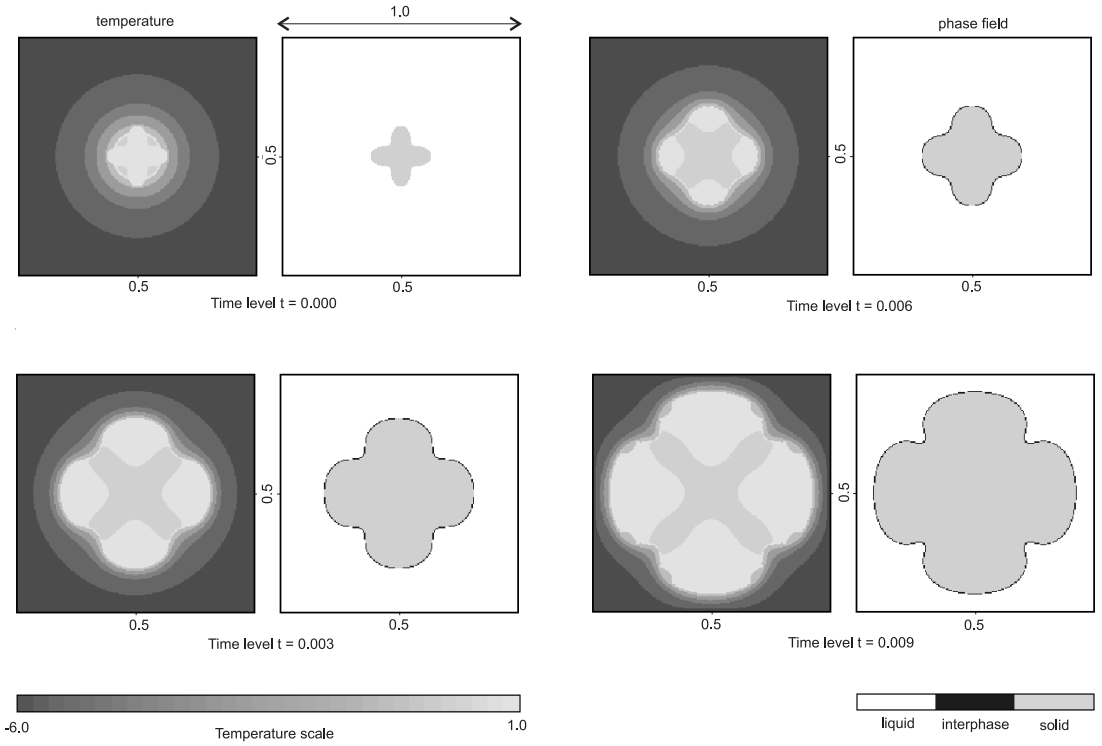

Figure 1.1: Single-crystal isotropic growth; parameters: $L = 6.0$, $\beta = 25.0$, $a = 4.0$, $\alpha = 1.0$, $L_1 = L_2 = 1.0$, $u(0) = -6.0$, $\xi = 0.0025$, $\Delta t = 0.0015$, $N_T = 6$, $N_1 = N_2 = 400$.

1 Introduction

The solidification of crystallic substances is accompanied by formation of microstructures as a result of self-organization of particles in the solid part of the material. Simulation of such phenomena and related mathematical aspects are in the scope of researchers for certain time, as their understanding contributes to the development of new, especially material technologies. The classical solidification model based on the Stefan problem is modified using the isotropic Gibbs-Thompson law relating the interface undercooling, curvature and normal velocity.

$$\begin{aligned} \frac{\partial u}{\partial t} &= \Delta u \quad \text{in } \Omega_s \text{ and } \Omega_l, && (1.1)\\ u\big|_{\partial\Omega} = 0, &\qquad u\big|_{t=0} = u_0, \\ \left.\frac{\partial u}{\partial n_\Gamma}\right|_s - \left.\frac{\partial u}{\partial n_\Gamma}\right|_l &= L v_\Gamma \quad \text{on } \Gamma(t), && (1.2)\\ F(u) &= -\kappa - \alpha v_\Gamma \quad \text{on } \Gamma(t), && (1.3)\\ \Omega_s(t)\big|_{t=0} &= \Omega_{so}, \end{aligned}$$

where Ω_s, Ω_l are solid and liquid phases, respectively, melting point is 0, u temperature field. Discontinuity of heat flux on $\Gamma(t)$ is described by the Stefan condition (1.2), where v_Γ is the velocity in the direction of the outer normal $\mathbf{n}_\Gamma$ to Ω_s, and L is the latent

heat. The formula (1.3) is the Gibbs-Thompson relation on $\Gamma(t)$ whose mean curvature is denoted as κ. F is related to the interface undercooling. The parameter α is the coefficient of attachment kinetics. Applied mathematical treatment of this problem lead to the use of various numerical techniques which were more or less able to produce relatively complex crystallic morphology. Here, we mention the use of adaptive BEM in [20], levelset methods in [18], [12], front tracking and FEM in [17], [13], variational methods in [1]. The presented work is related to the phase-field approach used within the context in question e.g. in [15], [8], [4], [5]. The system of equations analysed in [6] reads as:

$$\begin{aligned} \frac{\partial u}{\partial t} &= \Delta u + L\chi'(p)\frac{\partial p}{\partial t}, \\ \alpha\xi^2\frac{\partial p}{\partial t} &= \xi^2\Delta p + f_0(p) + F(u)\xi^2|\nabla p|, \end{aligned} \tag{1.4}$$

with initial conditions

$$u|_{t=0} = u_0\ , \quad p|_{t=0} = p_0,$$

and with boundary conditions of Dirichlet type

$$u|_{\partial\Omega} = 0\ , \quad p|_{\partial\Omega} = 0,$$

Here, $\xi > 0$ is the "small" parameter, and f_0 derivative of a double-well potential. The coupling function $F(u)$ is bounded and continuous, or even Lipschitz-continuous, $|.|$ denotes the Euclidean norm in $\mathbb{R}^n$. We consider $f_0(p) = ap(1-p)(p-\frac{1}{2})$ with $a > 0$. The enthalpy is given by $\mathcal{H}(u) = u - L\chi(p)$, where the coupling function χ is monotone with bounded, Lipschitz-continuous derivative: $\chi(0) = 0$, $\chi(0.5) = 0.5$, $\chi(1) = 1$, $supp(\chi') \subset< 0, 1 >$. For the sake of simplicity, $n = 2$, Ω is a bounded domain in $\mathbb{R}^n$ with a C^2 boundary, and boundary conditions are homogeneous. Obviously, the extension to higher dimensions, and to other boundary conditions is possible.

The above cited results concern isotropic models (see Figure 1.1), or models with weak anisotropy in the sense that the graph of surface energy density is strictly convex, which is the case for many metals. The crystalline case, when the strict convexity condition is no more valid, was treated e.g. in [19], [3], [2], [14]. We use the results of [3], where the Finsler geometry was introduced into the anisotropic motion by mean curvature, which is the special subproblem related to (1.1-1.3). Consequently, the Gibbs-Thompson law holds in the direction of Cahn-Hoffman vector ([11]). Our aim is to extent such approach to the solidification model, to show basic mathematical properties, and to perform computational studies demonstrating behaviour of the anisotropic model.

2 Equations

Before introducing the anisotropic form of equations, we give a brief summary of the Finsler-geometry concept, which seems to be a natural way of introducing anisotropy into the model in question. We stress out that details about this approach can be found in [3] and in references therein.

A nonnegative function $\Phi : \mathbb{R}^n \to \mathbb{R}^+$ which is smooth, strictly convex, $\mathcal{C}^2(\mathbb{R}^n - \{\Theta\})$ and satisfies:

$$\begin{aligned} \Phi(t\eta) &= |t|\Phi(\eta), \quad t \in \mathbb{R}, \eta \in \mathbb{R}^n, \\ \lambda|\eta| &\leq \Phi(\eta) \leq \Lambda|\eta|, \end{aligned}$$

where $\lambda, \Lambda > 0$, is called Finsler metric. The function given by

$$\Phi^0(\eta^*) = \sup\{\eta^* \cdot \eta \mid \Phi(\eta) \leq 1\},$$

is called dual Finsler metric. They satisfy the following relations

$$\begin{aligned} \Phi^0_\eta(t\eta^*) = \frac{t}{|t|}\Phi^0_\eta(\eta^*) \quad , \quad \Phi^0_{\eta\eta}(t\eta^*) = \frac{1}{|t|}\Phi^0_{\eta\eta}(\eta^*), \quad t \in \mathbb{R} - \{0\}, \\ \Phi(\eta) = \Phi_\eta(\eta) \cdot \eta \quad , \quad \Phi^0(\eta^*) = \Phi^0_\eta(\eta^*) \cdot \eta^*, \quad \eta, \eta^* \in \mathbb{R}^n, \end{aligned}$$

where the index η means derivative with respect to. We define the map $T^0 : \mathbb{R}^n \to \mathbb{R}^n$ as

$$\begin{aligned} T^0(\eta^*) &:= \Phi^0(\eta^*)\Phi^0_\eta(\eta^*) \text{ for } \eta^* \neq 0, \\ T^0(0) &:= 0. \end{aligned}$$

It allows to define the Φ-gradient of a smooth function u:

$$\nabla_\Phi u := T^0(\nabla u) = \Phi^0(\nabla u)\Phi^0_\eta(\nabla u).$$

Normal vector and velocity of a levelset of a field p

$$\Gamma(t) = \{\mathbf{x} \in \mathbb{R}^n \mid p(t, \mathbf{x}) = const.\} :$$

are

$$\mathbf{n}_{\Gamma,\Phi} = -\frac{\nabla_\Phi p}{\Phi^0(\nabla p)} = -\frac{T^0(\nabla p)}{\Phi^0(\nabla p)}, \quad v_{\Gamma,\Phi} = \frac{p_t}{\Phi^0(\nabla p)}.$$

The anisotropic curvature is give by the formula

$$\kappa_{\Gamma,\Phi} = div(\mathbf{n}_{\Gamma,\Phi}).$$

Compared to [3], we do not consider an explicit dependence of Φ on space, for the sake of simplicity.

Consequently, we can investigate an anisotropic motion by mean curvature

$$\alpha v_{\Gamma,\Phi} = -\kappa_{\Gamma,\Phi} + F,$$

in the direction of Cahn-Hoffmann vector $\mathbf{n}_{\Gamma,\Phi}$. Manifold described as

$$\Gamma(t) = \{\mathbf{x} \in \mathbb{R}^n \mid p(t, \mathbf{x}) = 0.5\},$$

with convention

$$\Omega_s(t) = \{\mathbf{x} \in \mathbb{R}^n \mid p(t, \mathbf{x}) > 0.5\}$$

induces the Hamilton-Jacobi equation

$$\alpha\frac{\partial p}{\partial t} = \Phi^0(\nabla p)\nabla\cdot(\frac{\nabla_\Phi p}{\Phi^0(\nabla p)}) + \Phi^0(\nabla p)F,$$

in analogy with isotropic case

$$\alpha\frac{\partial p}{\partial t} = |\nabla p|_E\nabla\cdot(\frac{\nabla p}{|\nabla p|_E}) + |\nabla p|_E F.$$

Similarly, we derive a modified (see (1.4)) anisotropic Allen-Cahn equation for curve dynamics in plane

$$\alpha\xi^2\partial_t p = \xi^2\nabla\cdot T^0(\nabla p) + f_0(p) + F\xi^2\Phi^0(\nabla p). \tag{2.1}$$

Example. We typically use the Finsler dual metric set as

$$\Phi^0(\eta^*) = \varrho\Psi(\Theta), \tag{2.2}$$

where $[\varrho,\Theta]$ are polar coordinates of η^*. Our choice is $\Psi(\Theta) = 1 + A\sin(m\Theta)$, where A is the anisotropy strength, and m the order of symmetry. The convexity condition reads as $A \le \frac{1}{1-m^2}$.

Finally, we establish an anisotropic phase-field model of solidification, using (1.4),

$$\begin{aligned}\frac{\partial u}{\partial t} &= \nabla^2 u + L\chi'(p)\frac{\partial p}{\partial t},\\ \alpha\xi\frac{\partial p}{\partial t} &= \xi\nabla\cdot T^0(\nabla p) + \frac{1}{\xi}f_0(p) + F(u)\xi\Phi^0(\nabla p),\end{aligned} \tag{2.3}$$

with boundary and initial conditions as in (1.4). We notice that the forcing term can include another type of anisotropy given by different dual Finsler metric: $F(u)\xi\Phi^1(\nabla p)$, as indicated by experiment - [16].

3 Theoretical results

First, we introduce the following notations:

$$(u,v) = \int_\Omega u(x)v(x)\,dx,\ \|u\| = \sqrt{\int_\Omega u(x)^2dx} \text{ for } u,v\in \mathrm{L}_2(\Omega),$$

$$(\nabla u,\nabla v) = \int_\Omega \nabla u(x)\cdot\nabla v(x)\,dx,\ \|\nabla u\| = \sqrt{\int_\Omega |\nabla u(x)|^2dx} \text{ for } u,v\in \mathrm{H}_0^1(\Omega).$$

We also notice that the assumptions on χ imply that there are constants $C_\chi, L_\chi > 0$ such that $|\chi'(s)| \le C_\chi, |\chi'(s_1)-\chi'(s_2)| \le L_\chi|s_1-s_2|$ for all $s,s_1,s_2\in\mathbb{R}$. Similarly, the assumptions on F imply that there are constants $C_F, L_F > 0$ such that $|F(s)| \le C_F, |F(s_1)-F(s_2)| \le L_F|s_1-s_2|$ for all $s,s_1,s_2\in\mathbb{R}$. We define the notion of the weak solution as usual in:

Definition 1 *Let $\Omega \subset \mathbb{R}^n$ be a bounded domain with Lipschitz-continuous boundary. Weak solution of the boundary-value problem with homogeneous Dirichlet boundary conditions for the phase-field equations (2.3) is a couple of functions $[u,p]$ from $(0,T)$ to $[\mathrm{H}_0^1(\Omega)]^2$ such that it satisfies*

$$\begin{aligned} \frac{d}{dt}(u - L\chi(p), v) + (\nabla u, \nabla v) &= 0 \text{ a.e. in } (0,T), \\ u|_{t=0} &= u_0, \\ \alpha\xi^2 \frac{d}{dt}(p,q) + \xi^2(T^0(\nabla p), \nabla q) &= (f_0(p), q) + \xi^2(F(u)\Phi^0(\nabla p), q) \text{ a.e. in } (0,T), \\ p|_{t=0} &= p_0. \end{aligned} \tag{3.1}$$

for each $v, q \in \mathrm{H}_0^1(\Omega)$.

The continuous imbedding of $\mathrm{H}^1(\Omega)$ into $\mathrm{L}_s(\Omega)$ for each $s \in (1, +\infty)$ ($\dim \Omega = 2$) ensures that $f_0(p) \in \mathrm{L}_2(\Omega)$ for almost all $t \in (0,T)$. If $[u,p] \in [\mathrm{L}_\infty(0,T;\mathrm{H}_0^1(\Omega))]^2$ solves (3.1), then $[u,p]$ is a continuous mapping from $\langle 0,T\rangle$ to $[\mathrm{H}^{-1}(\Omega)]^2$. Thus, the definition has proper sense. Our existence and uniqueness result is contained in the following theorem. The proof by its virtue contains the investigation of convergence of a semi-discrete scheme based on the Faedo-Galerkin method.

Theorem 1 *Consider the problem (3.1) in a bounded domain $\Omega \subset \mathbb{R}^2$ with a C^2 boundary, and with F being a bounded continuous function, χ a function with $\chi(0) = 0, \chi(1) = 1, \chi(0.5) = 0.5$, χ' bounded, Lipschitz continuous with the support in $\langle 0,1\rangle$. Assume that $\xi > 0$ is fixed, and*

$$u_0, p_0 \in \mathrm{H}^1(\Omega). \tag{3.2}$$

Then, there is a solution of the problem (3.1) satisfying

$$u, p \in \mathrm{L}_\infty(0,T;\mathrm{H}_0^1(\Omega)),\ p \in \mathrm{L}_2(0,T;\mathrm{H}^2(\Omega)),$$
$$\frac{\partial u}{\partial t}, \frac{\partial p}{\partial t} \in \mathrm{L}_2(0,T;\mathrm{L}_2(\Omega)).$$

Additionally, if F is Lipschitz-continuous, $\chi' \equiv 1$, and T^0 is strictly monotone, the solution is unique.

Proof. Here, we sketch main points of the proof, which follow the results of [6] and [7]. We derive a sequence of approximate solutions $[u^m, p^m]$ to the original problem. Assume that there is an orthonormal basis of the Hilbert space $\mathrm{L}_2(\Omega)$ denoted as $\{v_i\}_{i\in\mathbb{N}}$ where $(\forall i \in \mathbb{N})(v_i \in \mathrm{H}_0^1(\Omega))$. Let $V_m = span\{v_i\}_{i\in\mathbb{N}_m}$ be a finite-dimensional subspace ($\mathbb{N}_m = \{1,\dots,m\}$); $\mathcal{P}_m : \mathrm{L}_2(\Omega) \to V_m$ be the projection operator. Then, $[u^m, p^m]$ is obtained from

$$\begin{aligned} \frac{d}{dt}(u^m - L\chi(p^m), v) + (\nabla u^m, \nabla v) &= 0 \text{ a.e. in } (0,T),\ \forall v \in V_m, \\ u^m(0) &= \mathcal{P}_m u_0, \\ \alpha\xi^2 \frac{d}{dt}(p^m, q) + \xi^2(T^0(\nabla p^m), \nabla q) &= (f_0(p^m), q) + \xi^2(F(u^m)\Phi^0(\nabla p^m), q) \\ &\quad \text{a.e. in } (0,T),\ \forall q \in V_m, \\ p^m(0) &= \mathcal{P}_m p_0, \end{aligned} \tag{3.3}$$

and is defined for $t \in \langle 0, T_m)$. The *a priori* estimates bellow show the independence of T_m on m.

Multiplication by derivatives yields the energy equalities

$$\|\partial_t u^m\|^2 + \frac{1}{2}\frac{d}{dt}\|\nabla u^m\|^2 = L(\partial_t \chi(p^m), \partial_t u^m),$$
$$\alpha\xi^2\|\partial_t p^m\|^2 + \frac{\xi^2}{2}\frac{d}{dt}\Phi^0(\nabla p^m)^2 = (f_0(p^m), \partial_t p^m) + \xi^2(F(u^m)\Phi^0(\nabla p^m), \partial_t p^m),$$

and a priori estimates

$$\|\partial_t u^m\|^2 + \frac{d}{dt}\|\nabla u^m\|^2 \le L^2 C_\chi^2 \|\partial_t u^m\|^2, \tag{3.4}$$
$$\frac{1}{2}\alpha\xi^2\|\partial_t p^m\|^2 + \frac{\xi^2}{2}\frac{d}{dt}\Phi^0(\nabla p^m)^2 + \frac{d}{dt}(w_0(p^m), 1) \le \frac{C_F^2}{2\alpha}\xi^2\Phi^0(\nabla p^m)^2,$$

where $w_0' = -f_0$, $|F(u)| \le C_F$, $|\chi'(p)| \le C_\chi^2$. This implies that we are able to pass to the limit in (3.3), as

1. $\nabla p^{m'}$ converges strongly in $\mathrm{L}_2(0,T;\mathrm{L}_2(\Omega))$ to ∇p (by compact imbedding and testing by $p^{m'} - p$), $\nabla u^{m'}$ converges weakly in $\mathrm{L}_2(0,T;\mathrm{L}_2(\Omega))$ to ∇u,
2. $f_0(p^{m'})$ converges strongly in $\mathrm{L}_2(0,T;\mathrm{L}_2(\Omega))$ to $f_0(p)$ (polynomial nonlinearity), $\chi(p^{m'})$ converges strongly to $\chi(p)$ in $\mathrm{L}_2(0,T;\mathrm{L}_2(\Omega))$,
3. $\mathcal{P}_{m'}p_0$, $\mathcal{P}_{m'}u_0$ converge strongly to p_0, u_0 in $\mathrm{L}_2(\Omega)$,
4. $p^{m'}(0) = \mathcal{P}_{m'}p_0$, $u^{m'}(0) = \mathcal{P}_{m'}u_0$.

In addition, we observe that the function p belongs to $\mathrm{L}_2(0,T;\mathrm{H}_0^1(\Omega) \cap \mathrm{H}^2(\Omega))$, and that the weak solution satisfies the initial condition.

The uniqueness of the weak solution is shown using the Lipschitz continuity of F, strong monotonicity of T^0 (i.e. strict convexity of anisotropy), and the Gronwall lemma. □

4 Asymptotical behaviour

This section is devoted to a direct extension of results described in [4], which were inspired by [9]. A priori estimates imply that the energy functional

$$E_\xi[p_\xi](t) = \int_\Omega [\xi\frac{1}{2}\Phi^0(\nabla p_\xi)^2 + \frac{1}{\xi}w_0(p_\xi)]dx,$$

is bounded as

$$E_\xi[p_\xi](t) \le E_\xi[p_\xi](0)\exp\{\frac{C_F^2}{2\alpha}t\} \quad t \in (0,T),$$

where p_ξ is second component of the solution of (3.1). From [4], there is an estimate for the time derivative by

$$\frac{1}{2}\alpha\xi\int_0^T \|\partial_t p_\xi\|^2 dt + E_\xi[p_\xi](T) \le C_T E_\xi[p_\xi](0).$$

This allows to state the following theorem:

Theorem 2 *Let $[u_\xi, p_\xi]$ is the solution of (3.1) with the initial data satisfying $E_\xi[p_\xi](0) < M_0$ independently on ξ, and let*

$$\int_\Omega |p_\xi(0,\mathbf{x}) - v_0(\mathbf{x})| d\mathbf{x} \to 0,$$

as $\xi \to 0$, for a function $v_0 \in \mathrm{L}_1(\Omega)$. Then for any sequence ξ_n tending to 0 there is a subsequence $\xi_{n'}$ such that

$$\lim_{\xi_{n'} \to 0} p_{\xi_{n'}}(t,\mathbf{x}) = v(t,\mathbf{x}),$$

is defined a.e. in $(0,T) \times \Omega$. The function v reaches values 0 and 1, and satisfies

$$\int_\Omega |v(t_1,\mathbf{x}) - v(t_2,\mathbf{x})| d\mathbf{x} \le C|t_2 - t_1|^{\frac{1}{2}},$$

where $C > 0$ is a constant, and

$$\sup_{t \in <0,T>} \int_\Omega |\nabla v|_E d\mathbf{x} \le C_1,$$

in the sense of $BV(\Omega)$, where $C_1 > 0$ is a constant. The initial condition is

$$\lim_{t \to 0_+} v(t,\mathbf{x}) = v_0(\mathbf{x}),$$

a.e.

Matching procedure known from [10] can be used in recovering of the Gibbs-Thompson law

$$\alpha v_{\Gamma,\Phi} = -\kappa_{\Gamma,\Phi} + F + \mathcal{O}(\xi^2).$$

Details exceed the scope of this article. We also observe, that the phase equation in (2.3) is independent on particular form of the double-well potential w_0 (as it is in (1.4)), in difference to the Allen-Cahn equation (see [3], [10]).

5 Computational results

This section contains a summary of computational results obtained by the model using the equations (2.3). Numerical algorithm of the method of lines uses the FDM space discretisation on an uniform grid, and higher order time solvers such as Runge-Kutta-Mersn scheme. Detailed analysis and convergence results can be found in [4].

We introduce the following notations:

$$\mathbf{h} = (h_1, h_2)\,,\ h_1 = \frac{L_1}{N_1},\ h_2 = \frac{L_2}{N_2},$$

$$\mathbf{x}_{ij} = [x^1_{ij}, x^2_{ij}],\ u_{ij} = u(\mathbf{x}_{ij}),$$

$$\omega_\mathbf{h} = \{[ih_1, jh_2] \mid i = 1,\ldots,N_1 - 1;\ j = 1,\ldots,N_2 - 1\},$$

$$\bar{\omega}_\mathbf{h} = \{[ih_1, jh_2] \mid i = 0,\ldots,N_1;\ j = 0,\ldots,N_2\},\ \gamma_\mathbf{h} = \bar{\omega}_\mathbf{h} - \omega_\mathbf{h},$$

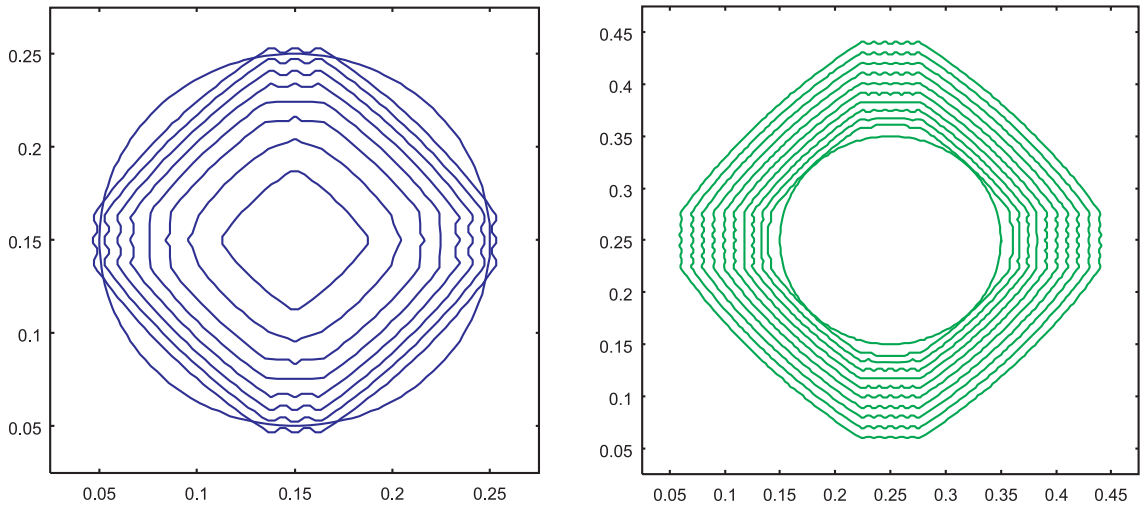

Figure 4.1: Anisotropic mean-curvature flow - initially circular curve ($r_0 = 0.1$) shrinks (left - forcing $F = 0.0$), or expands (left - forcing $F = -11.0$). The parameters of simulation are: $\xi = 0.012$, $a = 4.0$, $\alpha = 1.0$, $m = 4$, $A = 0.2$, $L_1 = L_2 = 0.3$, $N_1 = N_2 = 50$, $\Delta t = 0.001$.

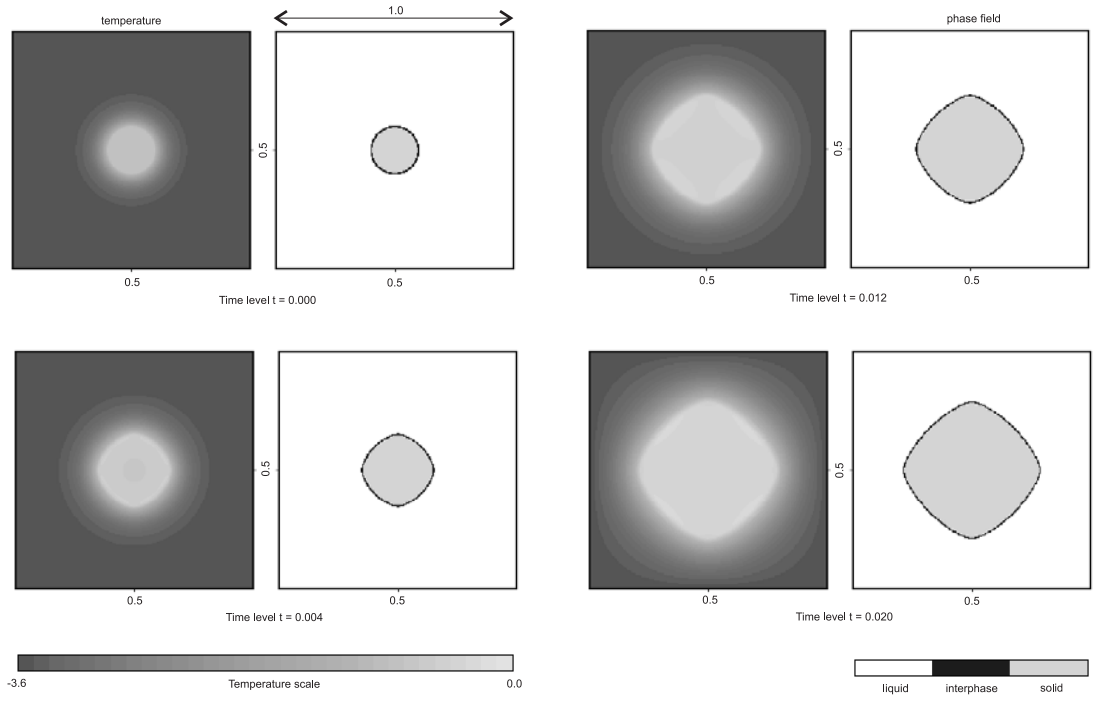

Figure 4.2: Single-crystal anisotropic growth with convex anisotropy; parameters: $L = 6.0$, $\beta = 25.0$, $a = 4.0$, $\alpha = 1.0$, $m = 4$, $A = 0.05$, $\xi = 0.01$, $u(0) = -6.0$, $L_1 = L_2 = 1.0$, $\Delta t = 0.004$, $N_T = 5$, $N_1 = N_2 = 200$.

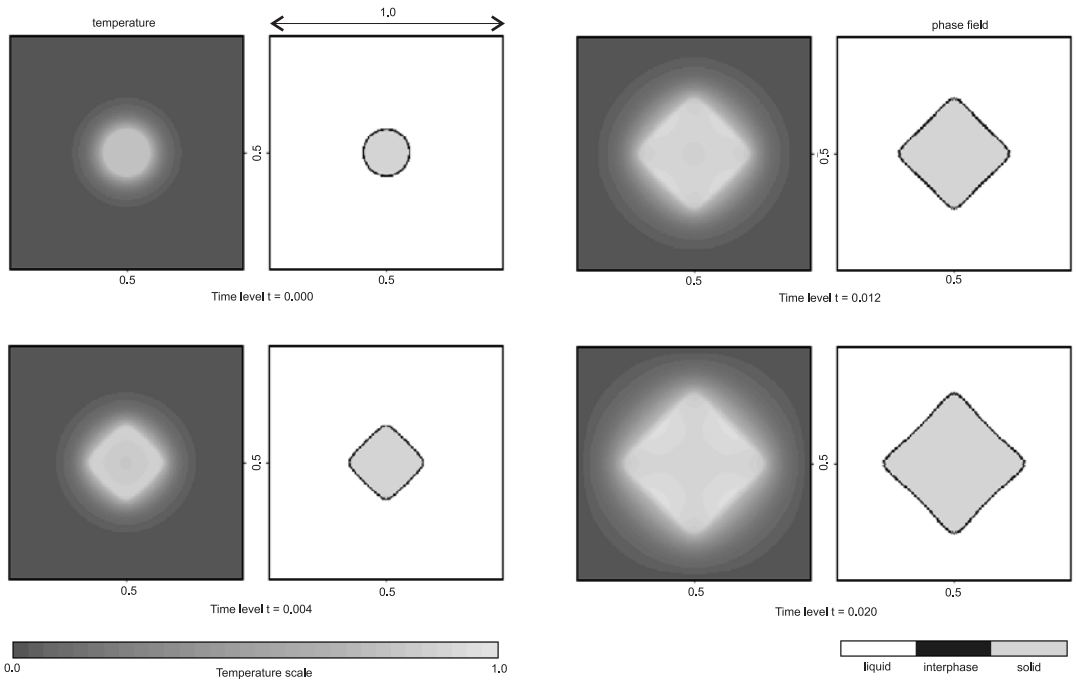

Figure 4.3: Single-crystal anisotropic growth with non-convex anisotropy; parameters: $L = 6.0$, $\beta = 25.0$, $a = 4.0$, $\alpha = 1.0$, $m = 4$, $A = 0.2$, $\xi = 0.01$, $u(0) = -6.0$, $L_1 = L_2 = 1.0$, $\Delta t = 0.003$, $N_T = 5$, $N_1 = N_2 = 200$.

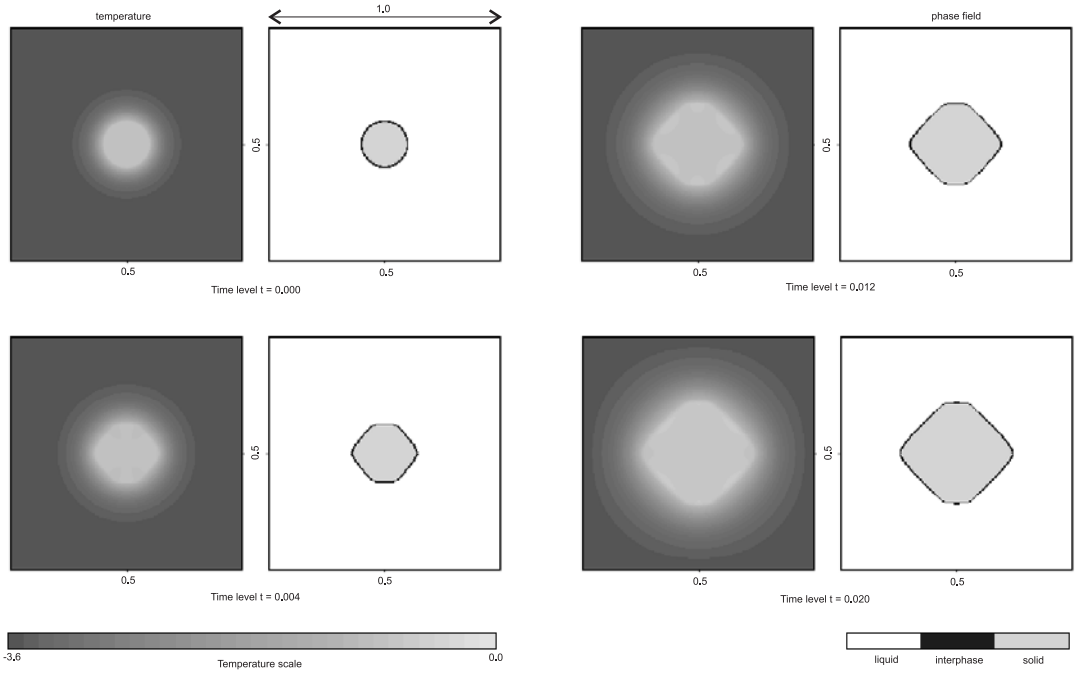

Figure 4.4: Single-crystal anisotropic growth with non-convex anisotropy; parameters: $L = 6.0$, $\beta = 25.0$, $a = 4.0$, $\alpha = 1.0$, $m = 6$, $A = 0.1$, $\xi = 0.01$, $u(0) = -6.0$, $L_1 = L_2 = 1.0$, $\Delta t = 0.003$, $N_T = 5$, $N_1 = N_2 = 200$.

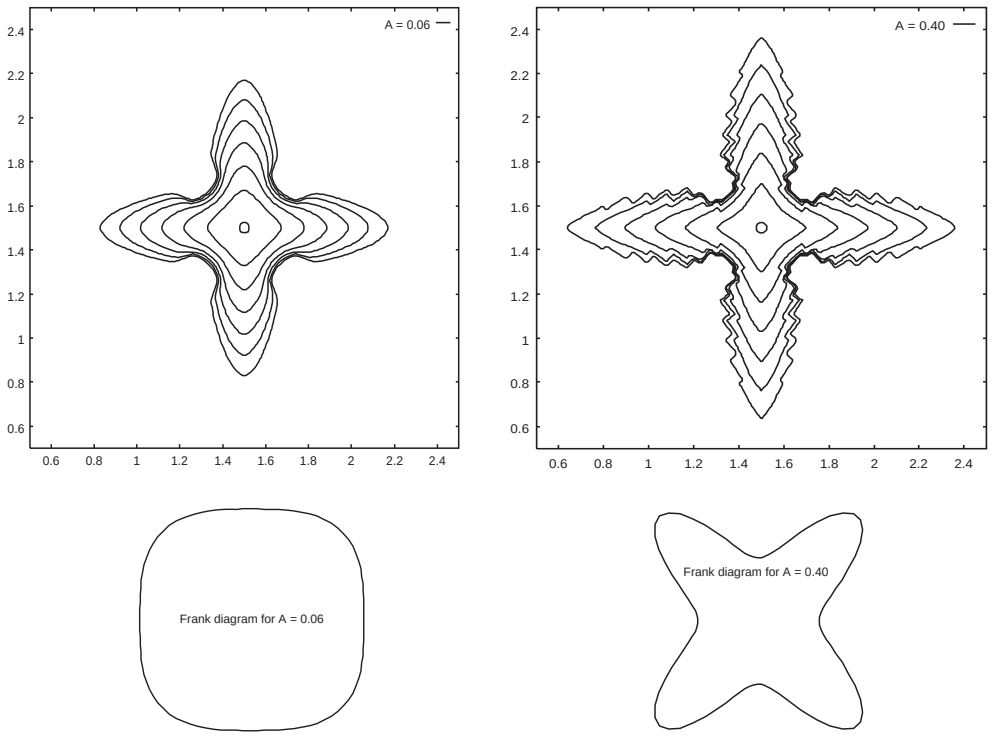

Figure 4.5: Qualitative study of dendritic growth for convex ($A = 0.06$) and non-convex anisotropy ($A = 0.40$). Other parameters are: $r = 2$, $\xi = 0.02$, $u^* = 1.0$, $u_0 = 0.0$, $L = 2.0$, $\beta = 300$, $a = 4.0$, $\alpha = 3$, $L_1 = L_2 = 3.0$, $N_1 = N_2 = 200$, $\Delta t = 0.008$, initial radius $= 0.025$.

$$
\begin{aligned}
u_{\bar{x}_1,ij} &= \frac{u_{ij} - u_{i-1,j}}{h_1} \quad , \quad u_{x_1,ij} = \frac{u_{i+1,j} - u_{ij}}{h_1}, \\
u_{\bar{x}_2,ij} &= \frac{u_{ij} - u_{i,j-1}}{h_2} \quad , \quad u_{x_2,ij} = \frac{u_{i,j+1} - u_{ij}}{h_2}, \\
u_{\bar{x}_1 x_1,ij} &= \frac{1}{h_1^2} \left(u_{i+1,j} - 2u_{ij} + u_{i-1,j}\right),
\end{aligned}
$$

and

$$
\bar{\nabla}_h u = [u_{\bar{x}_1}, u_{\bar{x}_2}], \quad \nabla_h u = [u_{x_1}, u_{x_2}], \quad \Delta_h u = u_{\bar{x}_1 x_1} + u_{\bar{x}_2 x_2}.
$$

The semi-discrete scheme has the form

$$
\begin{aligned}
&\dot{u}^h = D_0 \Delta_h u^h + L\chi'(p^h)\dot{p}^h \text{ on } \omega_{\mathbf{h}}, \\
&\quad u^h \mid_{\gamma_{\mathbf{h}}} = 0, \quad u^h(0) = \mathcal{P}_h u_0, \\
&\alpha\xi^2 \dot{p}^h = \xi^2 \nabla_h \cdot T^0(\bar{\nabla}_h p^h) + f_0(p^h) + \xi^2 \Phi^0(\nabla_h p^h) F(u^h) \text{ on } \omega_{\mathbf{h}}, \\
&\quad p^h \mid_{\gamma_{\mathbf{h}}} = 0, \quad p^h(0) = \mathcal{P}_h p_0,
\end{aligned}
$$

where its solution is a map $u^h, p^h :< 0, T > \rightarrow \mathcal{H}_{\mathbf{h}}$ and $\mathcal{P}_h : \mathcal{C}(\bar{\Omega}) \rightarrow \mathcal{H}_{\mathbf{h}}$ is a restriction operator.

We use a non-trivial coupling function

$$
\chi(p) = \begin{cases} 2^{2r-1} p^{2r} & \text{for } p < \dfrac{1}{2}, \\ 1 - 2^{2r-1}(1-p)^{2r} & \text{for } p \geq \dfrac{1}{2}, \end{cases}
$$

mostly with $r = 2$. We always set

$$
F(u) = \beta(u^* - u) \text{ for } |u - u^*| < C_u,
$$

and

$$
\begin{aligned}
F(u) &= -C_u \beta \text{ for } u \geq u^* + C_u, \\
F(u) &= C_u \beta \text{ for } u \leq u^* - C_u,
\end{aligned}
$$

in order to satisfy basic theoretical requirements imposed on F. If C_u is sufficiently large, the model behaves as if F were linear, and is applicable in real situations. The Finsler dual metric is set according to (2.2).

Our results are always in 2D, and show the solution for convex anisotropies, where our theory is valid. In addition, the model is able to treat even non-convex anisotropies. Figure 4.1 shows how a circle evolves according to the anisotropic mean-curvature flow given by Finsler geometry (2.1). As the anisotropy is non-convex, we observe the presence of wrinkles in "forbidden" directions, which depend on the numerical mesh. Figure 4.2 shows a single pattern growth under a convex anisotropy. Figures 4.3 and 4.4 have the same parameters, only the anisotropy is non-convex. Again, we observe wrinkling of phase boundaries, and almost flat parts corresponding to facets. Figure 4.5 compares a single-dendrite growth with identical physical and numerical setting, and with convex and non-convex anisotropies. We observe formation of corners and almost flat parts of phase boundary in the non-convex case.

Acknowledgement

The author was partially supported by the project No. J04/98/210000010 of the Ministry of Education of the Czech Republic, and by the project of the Grant Agency of Czech Republic No. 201/00/0080.

Bibliography

[1] R. Almgren. Variational algorithms and pattern formation in dendritic solidification. *J. Comput. Phys.*, 106:337–354, 1993.

[2] S. Angenent and M.E. Gurtin. Multiphase thermomechanics with interfacial structure. 2. Evolution of an isothermal interface. *Arch. Rational Mech. Anal.*, 108:323–391, 1989.

[3] G. Bellettini and M. Paolini. Anisotropic motion by mean curvature in the context of Finsler geometry. *Hokkaido Math. J.*, 25:537–566, 1996.

[4] M. Beneš. *Phase-Field Model of Microstructure Growth in Solidification of Pure Substances*. PhD thesis, Faculty of Nuclear Sciences and Physical Engineering, Czech Technical University, 1997.

[5] M. Beneš. Numerical simulation of microstructure growth in solidification by the phase–field model with a gradient coupling term. In R. Van Keer, R. Verhegghe, M. Hogge, and E. Noldus, editors, *ACOMEN'98, Advanced Computational Methods in Engineering*, pages 343–350, Maastricht, 1998.

[6] M. Beneš. Mathematical analysis of phase-field equations with numerically efficient coupling terms. Technical report, MMG 3-99, Department of Mathematics, FNSPE, Czech Technical University of Prague, 1999.

[7] M. Beneš. Anisotropic phase-field model of solidification - theory and simulation. In preparation, 2000.

[8] W.J. Boettinger, A.A. Wheeler, B.T. Murray, G.B. McFadden, and R. Kobayashi. Calculation of alloy solidification morphologies using the phase-field method. In T.S. Piwonka, V. Voller, and L. Katgerman, editors, *Modeling of Casting, Welding and Advanced Solidification Processes VI*, pages 79–86, 1993.

[9] L. Bronsard and R. Kohn. Motion by mean curvature as the singular limit of Ginzburg-Landau dynamics. *J. Differential Equations*, 90:211–237, 1991.

[10] G. Caginalp. An analysis of a phase field model of a free boundary. *Arch. Rational Mech. Anal.*, 92:205–245, 1986.

[11] J.W. Cahn and D.W. Hoffmann. A vector thermodynamics for anisotropic interfaces. 1. Fundamentals and applications to plane surface junctions. *Surface Sci.*, 31:368–388, 1972.

[12] S. Chen, B. Merriman, S. Osher, and P. Smereka. A simple level set method for solving Stefan problems. *J. Comp. Phys.*, 135:8–29, 1997.

[13] M. Fried. *Niveauflächen zur Berechnung zweidimensionaler Dendrite*. PhD thesis, Universität Freiburg, 1999.

[14] M.-H. Giga and Y. Giga. Evolving graphs by singular weighted curvature. *Arch. Rational Mech. Anal.*, 141:117–198, 1998.

[15] R. Kobayashi. Modeling and numerical simulations of dendritic crystal growth. *Physica D*, 63:410–423, 1993.

[16] M. Rappaz. Private communication. 1997.

[17] A. Schmidt. *Die Berechnung dreidimensionaler Dendriten mit Finiten Elementen*. PhD thesis, Universität Freiburg, 1993.

[18] J.A. Sethian and J. Strain. Crystal growth and dendritic solidification. *J. Comput. Phys.*, 98:231–253, 1992.

[19] J.E. Taylor. Motion of curves by crystalline curvature, including triple junctions and boundary points. *Proc. of Symposia in Pure Math.*, 54:417–438, 1993.

[20] E. Yokoyama and T. Kuroda. Pattern formation in growth of snow crystals occuring in the surface kinetics process and the diffusion process. *Phys. Rev. A*, 41:2038–2049, 1990.